Long-Range Spin-Triplet Helix in Proximity Induced Superconductivity in Spin-Orbit-Coupled Systems

Xin Liu, J. K. Jain, and Chao-Xing Liu

Long-Range Spin-Triplet Helix in Proximity Induced Superconductivity in Spin-Orbit-Coupled Systems

Xin Liu, J. K. Jain, and Chao-Xing Liu

Department of Physics, The Pennsylvania State University, University Park, Pennsylvania 16802-6300

(Dated: November 3, 2014)

We study proximity induced triplet superconductivity in a spin-orbit-coupled system, and show that the $\boldsymbol{d}$-vector of the induced triplet superconductivity undergoes precession that can be controlled by varying the relative strengths of Rashba and Dresselhaus spin-orbit couplings. In particular, a long-range spin-triplet helix is predicted when these two spin-orbit couplings have equal strengths. We also study the Josephson junction geometry and show that a transition between 0 and π junctions can be induced by controlling the spin-orbit coupling with a gate voltage. An experimental setup is proposed to verify these effects. Conversely, the observation of these effects can serve as a direct confirmation of triplet superconductivity.

Introduction - Crucial to the success of spintronics [1] are injection of spin, its long decay length and its manipulation. The study of spin transport in a superconductor has given rise to the subfield known as superconducting spintronics [2–4]. One may wonder if the spin-1 of Cooper pairs in a triplet superconductor can play a similar role as the electron spin in spintronics. The observation of surprisingly long-range proximity effect in a superconductor (SC)/ferromagnet (FM) junction [5–11] has been interpreted in terms of an injection into the FM of triplet Cooper pairs with a long decay length [12–17]. However, it is unclear how to manipulate the long-range part of the induced triplet pair.

We propose here a geometry in which the triplet pairs are injected into a material with spin-orbit coupling (SOC) and show, theoretically, that they can be manipulated by varying the relative strengths of the Rashba and Dresselhaus SOCs. In particular, we predict a long-range spin-triplet helix, which can be verified by observing a $0-\pi$ transition in Josephson junctions as a function of the SOC strengths. We show that the effect is robust against any spin independent scattering. Proximity effect in SOC materials has been considered previously,[18, 19] but with only Rashba SOC, which does not produce long-range effects discussed below.

Before presenting the detailed microscopic theory, we first illustrate the underlying physics, shown in Fig 1. In the absence of magnetization and SOC, four kinds of Cooper pairs (singlet $|\uparrow\downarrow\rangle - |\downarrow\uparrow\rangle$ and triplet pairs $|\uparrow\downarrow\rangle + |\downarrow\uparrow\rangle$, $|\uparrow\uparrow\rangle \pm |\downarrow\downarrow\rangle$) are allowed with a zero center-of-mass momentum. The magnetization breaks the degeneracy between $|k,\uparrow\rangle$ and $|-k,\downarrow\rangle$. It will lead to a spatially modulated oscillation $e^{-iqx}|\uparrow\downarrow\rangle \pm e^{iqx}|\downarrow\uparrow\rangle$ [20, 21] for the Cooper pairs with opposite spins but leave the pairs $|\uparrow\uparrow\rangle \pm |\downarrow\downarrow\rangle$ unchanged, as shown in Fig 1(b). (Here we assume that the system is uniform along y and z directions so that the center-of-mass momentum of pairs is always zero along these directions.) On the contrary, SOC breaks the degeneracy between $|k,\uparrow(\downarrow)\rangle$ and $|-k,\uparrow(\downarrow)\rangle$,

as shown in Fig. 1(c,d). Thus, the Cooper pairs with parallel spins will oscillate spatially as $e^{-iqx}|\uparrow\uparrow\rangle + e^{iqx}|\downarrow\downarrow\rangle$, while the pairs $|\uparrow\downarrow\rangle \pm |\uparrow\downarrow\rangle$ remain unchanged. Here we emphasize that the spin quantization axis aligns along different directions for different momenta, determined by the form of SOC in Fig. 1(c). The spatially oscillatory pairs will decay after taking into account all possible wave vectors of q [15] in the case of Fig. 1(b). Similarly, the triplet pairs $|\uparrow\uparrow\rangle$ and $|\downarrow\downarrow\rangle$ in Fig. 1(c) will also generally decay rapidly in the SOC region. Therefore, in the presence of magnetization and generic SOC, only the pairs with zero center-of-mass momenta exhibit long-range proximity effect. However, there is an exception for a system with equal strengths of Rashba and Dresselhaus SOCs. In this case, the Fermi surfaces for two spin bands shifted in opposite directions by $Q = 4m\alpha$, shown in Fig. 1(d). Here m being the electron effective mass and α being the Rashba SOC strength. Thus, all of spatially oscillatory pairs have the same wave vector Q and will not decay even in the presence of spin independent scattering. We show below that these oscillatory triplet pairs result in a long-range helical mode, dubbed "long-range spin-triplet helix", in analogy to the persistent spin helix observed in two dimensional electron gases (2DEGs)[22–26].

Hamiltonian and pairing functions - We study the SC/normal-conductor structure whose Hamiltonian takes the form

$$\hat{H} = \begin{pmatrix} H_0 & \hat{\Delta} \\ \hat{\Delta}^\dagger & -H_0^* \end{pmatrix}, \hat{\Delta} = \Delta(x)i\sigma_y,$$

$$H_0 = \left(\frac{\boldsymbol{p}^2}{2m} - \mu\right)\sigma_0 + (\boldsymbol{M}(x) + \boldsymbol{h}(x,\boldsymbol{k}))\cdot\boldsymbol{\sigma},$$

in the basis $[c_\uparrow, c_\downarrow, c_\uparrow^\dagger, c_\downarrow^\dagger]^{\mathrm{T}}$, where $c_{\uparrow,\downarrow}$ and $c_{\uparrow,\downarrow}^\dagger$ are electron annihilation and creation operators for different spins, m is the electron mass, μ is the chemical potential, $\hat{\Delta}$ is the spin-singlet s-wave superconducting gap, $\boldsymbol{M}$ is the magnetization, $\boldsymbol{h}$ is the effective magnetic field of SOC and $\boldsymbol{\sigma}$ denotes the spin operators. The gap strength
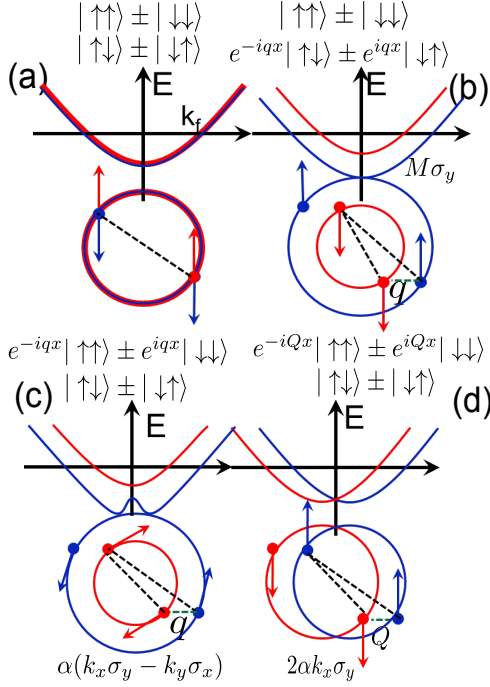
FIG. 1. Energy dispersion and Fermi surfaces are shown for (a) normal metals, (b) ferromagnets, (c) a 2DEG with Rashba SOC and (d) a 2DEG with equal strengths of Rashba and Dresselhaus SOCs. The possible forms of spin states of Cooper pairs, including singlet and triplet pairs, are also illustrated in the figures. For $k_y \neq 0, k_x = 0$, the gap between two spin bands in (c) is $|2\alpha k_y|$.

$\Delta(x)$ is zero in the proximity region and has a constant value Δ in the superconducting region. The magnetization $\boldsymbol{M}(x)$ and effective magnetic field of SOC $\boldsymbol{h}(x,k)$ are only present in the normal-conductor and depend on the spatial coordinate x shown in Fig. 2 and Fig. 3(a,b).

Cooper pairs in spin space can be described microscopically by a pairing function $f^R(E,\boldsymbol{r}) = (d_0\sigma_0 + \boldsymbol{d} \cdot \boldsymbol{\sigma})i\sigma_y$ [12, 27], which is the off diagonal block of the retarded Green's function

$$G^{\mathrm{R}}(E,\boldsymbol{r},\boldsymbol{r}')\big|_{\boldsymbol{r}=\boldsymbol{r}'} = \begin{pmatrix} g^{\mathrm{R}}(E,\boldsymbol{r}) & f^{\mathrm{R}}(E,\boldsymbol{r}) \\ \overline{f}^{\mathrm{R}}(E,\boldsymbol{r}) & \overline{g}^{\mathrm{R}}(E,\boldsymbol{r}) \end{pmatrix}. \quad (1)$$

Here d_0 and $\boldsymbol{d}$ are the expectation value of singlet and triplet pairs respectively, E is the energy, $\boldsymbol{r}$ and $\boldsymbol{r}'$ are the spatial coordinates; we have $f^{\mathrm{R}}_{ij}(E,\boldsymbol{r}) = -(\overline{f}^{\mathrm{R}}_{ij}(-E,\boldsymbol{r}))^{\dagger}$; and $g^{\mathrm{R}}(\overline{g}^{\mathrm{R}})$ is the electron (hole) Green's function. Both f^R and g^R are 2×2 matrices in spin space. The superconducting gap is related to the pairing function by the equality $\hat{\Delta} = (1/2\pi) \int dE\lambda f_E \mathrm{Im} f^{\mathrm{R}}$ where λ is the attractive interaction strength and f_E is the Fermi distribution. In the proximity region, the superconducting gap is zero because of $\lambda = 0$, but the pairing function f^{R} can be nonzero. Below, we will calculate, in the presence of either magnetization or SOC, the spatial evolution of
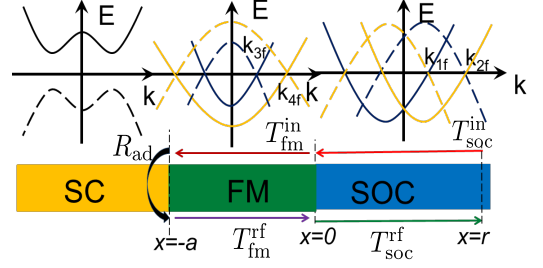

FIG. 2. A schematic plot of a SC/FM/SOC junction. Energy dispersions for different regions are shown above the junction structure. The colors in the dispersion relation represent different spin indices and the solid lines (dashed lines) denote electron (hole) bands. $k_{1(2),f}$ and $k_{3(4),f}$ are the Fermi momenta of different spin bands for SOC and FM regions, respectively. Different propagation or reflection processes are denoted by $T^{in(out)}_{fm(soc)}$ or R_{ad}.

the pairing function $f^R(E,\boldsymbol{r})$ in the proximity region and show its consistence to the physical picture in Fig. 1.

$\boldsymbol{d}$-vector in a 1D SC/FM/SOC junction - In the ferromagnetic region $(x \in (-a,0))$ the SOC is zero, while in the SOC region $(x > 0)$ the magnetization is zero shown in Fig. 2. In the SOC (FM) region, the Fermi wave vectors of the spin split bands, $k_{1\mathrm{f}}, k_{2\mathrm{f}}$ $(k_{3\mathrm{f}}, k_{4\mathrm{f}})$ in Fig 2, satisfy

$$k_{2\mathrm{f}} - k_{1\mathrm{f}} = \frac{2|\boldsymbol{h}(k_{\mathrm{f}})|}{\hbar v_{\mathrm{f}}}, \quad k_{4\mathrm{f}} - k_{3\mathrm{f}} = \frac{2M}{\hbar v_{\mathrm{f}}}, \quad (2)$$

with $\hbar v_{\mathrm{f}} = \hbar k_{\mathrm{f}}/m = \sqrt{2\mu/m}$, assuming $h, M \ll \mu$. The Green's functions G^R can be related to the reflection matrix R by the Fisher-Lee relation[28] which has been applied to the superconducting proximity effect [29, 30]. For 1D case, Fisher-Lee relation in the basis $[c_{\uparrow}, c_{\downarrow}, c_{\uparrow}^{\dagger}, c_{\downarrow}^{\dagger}]^{\mathrm{T}}$ takes the form [29–31]

$$R_{ij}(E,\boldsymbol{r}) = -\delta_{ij} + i\hbar\sqrt{v_i v_j}G^R_{ij}(E,\boldsymbol{r}), \quad (3)$$

where $i,j = 1,\ldots,4$ and $v_{i(j)}$ is the velocity of the particle at energy E in $i(j)$ channels. Therefore, we will calculate the reflection matrix to extract pairing functions in 1D case. For simplicity, we consider the clean limit with perfect transmission at FM/SOC boundary and ideal Andreev reflection at the FM/SC boundary. The reflection matrix $R(x)$ in the SOC region can be decomposed into five matrices representing five steps shown in Fig. 2: an electron first propagates from $x = r$ to the interface at $x = 0$ ($T^{\mathrm{in}}_{\mathrm{soc}}$); it then propagates to the interface at $x = -a$ ($T^{\mathrm{in}}_{\mathrm{fm}}$); ideal Andreev reflection occurs at the SC/FM interface of $x = -a$ (R_{ad}), where the electron is completely reflected as a hole; the reflected hole transmits back to $x = 0$ ($T^{\mathrm{rf}}_{\mathrm{fm}}$), and finally to the SOC region at $x = r$ ($T^{\mathrm{rf}}_{\mathrm{soc}}$) [32]. Consequently, the scattering matrix $R(r)$ takes the form

$$R(r) = T^{\mathrm{rf}}_{\mathrm{soc}} T^{\mathrm{rf}}_{\mathrm{fm}} R_{\mathrm{ad}} T^{\mathrm{in}}_{\mathrm{fm}} T^{\mathrm{in}}_{\mathrm{soc}}. \quad (4)$$

When there is no SOC (i.e., $r = 0$), the reflection matrix at FM/SOC boundary takes the form [32]

$$R(r=0) = T_{\text{fm}}^{\text{rf}} R_{\text{ad}} T_{\text{fm}}^{\text{in}} = -\hbar v_{\text{f}} (d_0 \sigma_0 + \boldsymbol{d} \cdot \boldsymbol{\sigma}) i \sigma_y \otimes \tau_y, \quad (5)$$

where

$$(d_0, \boldsymbol{d}) = -i \frac{e^{-i\alpha}}{\hbar v_{\text{f}}} \left(\cos\left(\frac{2Ma}{\hbar v_{\text{f}}}\right), i \sin\left(\frac{2Ma}{\hbar v_{\text{f}}}\right) \boldsymbol{m} \right), \quad (6)$$

$\boldsymbol{m} = \boldsymbol{M}/M$, $\alpha = \arccos(E/\Delta)$ and $\tau_z = +1(-1)$ for the electron (hole) in the Nambu space. In the limit $M \ll \mu$, we take $\sqrt{v_i v_j} \approx v_{\text{f}}$. Eqs. (5) and (6) show oscillation between singlet and triplet pairs as a function of a, the distance from the SC/FM interface. Thus, by choosing an appropriate length a of the FM region, one can use the SC/FM junction to inject singlet or triplet pairs into the SOC region.

When there is no FM ($a = 0$), the reflection matrix reduces to $R(r) = T_{\text{soc}}^{\text{rf}} R_{\text{ad}} T_{\text{soc}}^{\text{in}} = R_{ad}$ [32] in the SOC region. This is because SOC does not lift the degeneracy of time reversed pairs, as shown in Fig 1 (c) and (d). For an FM of length a satisfying $2Ma/\hbar v_{\text{f}} = \pi/2$, only triplet pairs with $\boldsymbol{d}$-vector along $\boldsymbol{M}$ are injected into the SOC region. When the effective magnetic field of SOC is parallel to the magnetization, say $\boldsymbol{h}(\boldsymbol{k}) \parallel \boldsymbol{M}$, the reflection matrix in the SOC region can be written as

$$R(r) = -e^{-i\alpha} \boldsymbol{m} \cdot \boldsymbol{\sigma} i \sigma_y \otimes \tau_y. \quad (7)$$

When $\boldsymbol{h}(\boldsymbol{k}) \perp \boldsymbol{M}$, the reflection matrix in the SOC regime has the form

$$R(r) = -\hbar v_{\text{f}} (d_1 \boldsymbol{m} \cdot \boldsymbol{\sigma} + d_2 \boldsymbol{m} \times \boldsymbol{n} \cdot \boldsymbol{\sigma}) i \sigma_y \otimes \tau_y, \quad (8)$$

where

$$(d_1, d_2) = \frac{e^{-i\alpha}}{\hbar v_{\text{f}}} \left(\cos(k_{2\text{f}} - k_{1\text{f}}) r, \sin(k_{2\text{f}} - k_{1\text{f}}) r \right), \quad (9)$$

and $\boldsymbol{n}$ is the unit direction of $\boldsymbol{h}(k_{\text{f}})$. Here d_1 and d_2 give the decomposition of the $\boldsymbol{d}$-vector along the direction $\boldsymbol{m}$ and $\boldsymbol{m} \times \boldsymbol{n}$, respectively. Eq. (7) implies that $\boldsymbol{d}$-vector keeps its original direction in the case of $\boldsymbol{d} \parallel \boldsymbol{h}(\boldsymbol{k})$. In contrast, Eq. (8) shows that in the case of $\boldsymbol{d} \perp \boldsymbol{h}(\boldsymbol{k})$, $\boldsymbol{d}$-vector precesses in the plane perpendicular to $\boldsymbol{h}(\boldsymbol{k})$ when propagating along 1D SOC region. The above conclusions are consistent with our physical picture shown in Fig 1(c,d). Especially, based on Eq (9), the precession of $\boldsymbol{d}$-vector leads to a helical structure, which is dubbed $\boldsymbol{d}$-helix or spin-triplet helix and schematically shown by red arrows in the SOC region of Fig 3 (b).

0 and π Josephson junction transition - To confirm the predicted $\boldsymbol{d}$-helix, we propose an experimental setup of a SC/FM/SOC/FM/SC junction (Fig. 3(a,b)) and show that the $\boldsymbol{d}$-helix can lead to a $0-\pi$ transition in Josephson junctions [15]. The magnetizations of two ferromagnetic layers point along x and $-x$ direction (Fig. 3(a,b)), to ensure a trivial 0-Josephson junction in the absence of
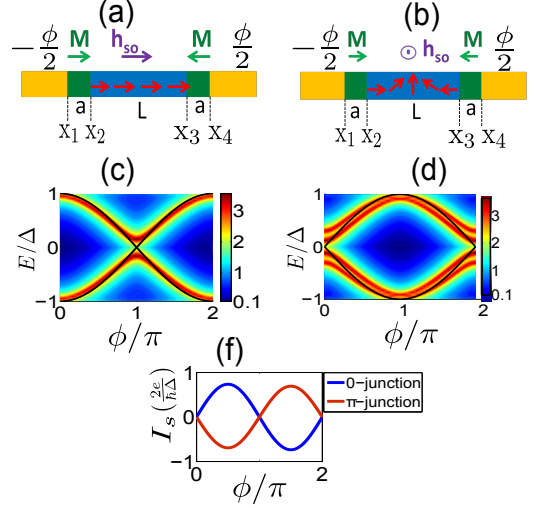

FIG. 3. The magnetization direction (the green arrows) and the effective magnetic field direction of SOC (the purple arrow) are shown (a) for a 0-junction and (b) a π-junction. The red arrows reveals the spatial distribution of d-vector. The phases of SCs at two sides are taken to be $\phi/2$ and $-\phi/2$. The color in (c) and (d) shows the spectral function of the SC/FM/SOC/FM/SC junction (logarithmic plot) as a junction of the relative phase ϕ for a 0-junction and π-junction, respectively. The black lines are the Andreev levels from analytical calculations. (f) shows the current-phase relation for the 0- and π-junction.

the SOC region. The lengths of FMs are chosen to satisfy $2Ma/\hbar v_{\text{f}} = \pi/2$, so only triplet pairs with $\boldsymbol{d}$-vector along x direction are injected into the SOC region.

We consider two cases with the SOC $\boldsymbol{h}(k) = \alpha k_x \hat{e}_x \parallel \boldsymbol{M}$ in Fig. 3(a) and $\boldsymbol{h}(k) = \alpha k_x \hat{e}_y \perp \boldsymbol{M}$ in Fig. 3(b). The length of the SOC wire satisfy $(k_{2\text{f}} - k_{1\text{f}})L = \pi$. To study the current-phase relation in this setup, we first calculate the Andreev levels numerically by evaluating the spectral function, $\text{Tr}[\sum_n g^R(E, x_n)]/N$, in a tight-binding model. Here g^R is the electron retarded Green's function defined in Eq. (1), x_n represents the nth site and N is the total number of sites in the proximity region. The spectral functions are plot as a function of the relative phase ϕ between two SCs in Fig. 3(c,d). The peaks shown by the red color indicate Andreev levels. We also obtain Andreev levels analytically using the standard scattering matrix method [32–34]. The analytical results are shown by two black lines in Fig 3(c,d), which are consistent with the numerical results. There is a small difference that the crossings of the black curves at $\phi = \pi$, in Fig. 3(c) and at $\phi = 0; 2\pi$ in Fig. 3(d) turn into anti-crossings in numerical results. This is because we impose a barrier potential at the SC/FM interfaces and include the Fermi velocity mismatch among different regions in numerical calculations, which remove all degeneracies in analytical results. The anti-crossing changes the period of the Josephson current at zero temperature, $I_s = \frac{2e}{\hbar} \sum_n \partial E_n / \partial \phi$ with

the summation of negative Andreev levels, from 4π (black curves) to 2π [33, 35]. The Josephson current for the Fig. 3(c) gives the form of $I_s \sim \sin(\phi)$ (the blue line in Fig. 3(f)), which corresponds to a 0-junction. In contrast, for the Fig. 3(d) we have $I_s \sim \sin(\phi + \pi)$ (the red line in Fig. 3(f)), indicating a π-junction. This 0-pi junction transition is consistent with the physical picture of the d-vector precession, shown by red arrows in Fig. 3(a,b). Further calculations show that the π junction is obtained for L satisfying $\pi/2 < (k_{1f} - k_{2f})L < 3\pi/2$ [36].

d-helix in a 2D system - Having clarified the physics in a 1D model, we next ask if **d**-helix also exists in a 2D system. For a 2DEG, the SOC has the form (assuming x-axis along [110] direction)

$$H_{\text{so}} = (\alpha + \beta)k_x\sigma_y + (\beta - \alpha)k_y\sigma_x,$$

where α and β are the Rashba and Dresselhaus SOC strengths. When $\alpha = \beta$, the Fermi surface with the spin parallel (anti-parallel) to the y axis is shifted along -x (x) direction by $Q/2$, as shown in Fig 1(d). As a result, the eigenenergies of two spin states satisfy $\epsilon_1(\mathbf{k}) = \epsilon_2(\mathbf{k} + \mathbf{Q})$, where $\mathbf{Q} = 4m\beta\hat{e}_x$, and 1 (2) denotes the spin parallel (anti-parallel) to the y axis. As shown in Refs. [22–26], one can construct *spin* helix operators, which commute with the Hamiltonian and lead to a persistent spin helix mode.

In our model with superconductivity, we can define triplet pairing operators

$$\hat{d}_x = \frac{1}{2}\left(\sum_{\{\mathbf{k},i\}} \delta(\epsilon_{\mathbf{k},i} - \mu)c_{\mathbf{k},i}^\dagger c_{-\mathbf{k}-(-1)^i\mathbf{Q},i}^\dagger + \text{h.c.}\right) \quad (10)$$

$$\hat{d}_z = \frac{1}{2i}\left(\sum_{\{\mathbf{k},i\}} \delta(\epsilon_{\mathbf{k},i} - \mu)c_{\mathbf{k},i}^\dagger c_{-\mathbf{k}-(-1)^i\mathbf{Q},i}^\dagger - \text{h.c.}\right) \quad (11)$$

where the summation is performed in the interval $\{\mathbf{k}, i\} = \{k_x < (-1)^i Q/2, k_y\}$ at the Fermi surface to avoid double counting. These two operators represent a **d**-helix of triplet pairs with center-of-mass Q in x-z plane. Since the operators $\hat{d}_{x,z}$ commute with the Hamiltonian $H_0 + H_{so}$ [32], a persistent **d**-helix also exists in the triplet superconducting proximity region. It is also noted that in the case of $\alpha = \beta$, the Hamiltonian even with a spin independent scattering potential, $H = H_0 + H_{so} + V(\mathbf{r})\sigma_0$, can be transformed to a Hamiltonian without SOC through the unitary matrix $U = \exp(-iQx/2)\sigma_y$. This is because U is independent on momenta and commutes with $V(\mathbf{r})\sigma_0$. At the same time, the triplet pairs with center-of-mass momentum Q as defined in Eq. (10, 11) is transformed to those with zero center-of-mass momentum as shown in Fig 1(a). Therefore, we expect that this spin-triplet helix is immune to any spin-independent scattering and its decay length should be as long as the Cooper pairs coherence length [33] in the normal region. This can be further confirmed by solving Usadel equations [37, 38] with SOCs [32].
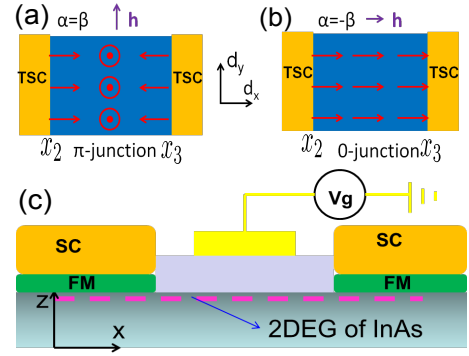

FIG. 4. The spatial dependence of **d**-vector of triplet pairs (the red arrows) and the corresponding effective magnetic field (the purple arrows) of the SOC are shown for (a) $\alpha = \beta$ (π-junction) and (b) $\alpha = -\beta$ (0-junction). TSC means triplet superconductor. (c) The proposed 2D SC/FM/SOC/FM/SC structure for an electronic-tunable Josephson junction.

In experiments, the Dresselhaus parameter β is fixed while Rashba parameter α can be tuned by a gate voltage. Therefore, the following geometry can be used to confirm the oscillatory triplet pairs by observing an electrically tunable 0-π transition. The length L of the SOC region is chosen to satisfy the condition $QL = \pi$. From the above discussion, when $\alpha = \beta$, the **d**-vector of triplet pairs changes its sign after propagating from $x = x_2$ to $x = x_3$ (Fig. 4(a)), leading to a π-junction. If we tune the Rashba parameter to $\alpha = -\beta$, the effective magnetic field of SOC $\mathbf{h} = 2\beta k_y\hat{e}_x$ is along the x direction, parallel to **d**-vector. Based on our theory, **d**-vector keeps its direction in the SOC region (Fig. 4(b)) and we will have a 0-junction. The proximity effect in the 2D Josephson junction for these two cases should be long-range according to our arguments. For realistic experiments, InAs quantum wells provide a potential candidate (Fig 4(c)), because they show strong proximity effect due to their low Schottky barrier [39]. If the two FM layer are Ni, 1 nm thickness [9] is enough to convert singlet pairs in SC to triplet pairs on FM/InAs interface. For the effective mass $m_{\text{eff}} 0.04m_e$ and typical $\alpha = 0.2\text{eV}\text{Å}$ in InAs quantum wells, we find $Q \approx 40\mu m^{-1}$, which corresponds to the length of $\sim 80nm$ of the SOC region to realize the Josephson $0 - \pi$ junction transition. This length is much smaller than the coherence length, $\xi_N = \hbar^2\sqrt{2\pi n}/m_{\text{eff}}2\pi k_B T_c \approx 4\mu m$ [33], where $n = 10^{12}\text{cm}^{-2}$ is the typical electron density in the InAs quantum well and $T_c = 1.2K$ is the critical temperature of Al.

[1] I. Zutic, J. Fabian, and S. Das Sarma, Rev. Mod. Phys. **76**, 323 (2004).

[2] K. Ohnishi, T. Kimura, and Y. Otani, Applied Physics Letters **96**, 192509 (2010).

[3] C. Quay, D. Chevallier, C. Bena, and M. Aprili, Nature Physics **9**, 84 (2013).

[4] T. Wakamura, N. Hasegawa, K. Ohnishi, Y. Niimi, and Y. Otani, Phys. Rev. Lett. **112**, 036602 (2014).

[5] R. Keizer, S. Goennenwein, T. Klapwijk, G. Miao, G. Xiao, and A. Gupta, NATURE **439**, 825 (2006).

[6] J. Wang, M. Singh, M. Tian, N. Kumar, B. Liu, C. Shi, J. K. Jain, N. Samarth, T. E. Mallouk, and M. H. W. Chan, NATURE PHYSICS **6**, 389 (2010).

[7] J. W. A. Robinson, J. D. S. Witt, and M. G. Blamire, Science (2010), 10.1126/science.1189246.

[8] T. S. Khaire, M. A. Khasawneh, W. P. Pratt, and N. O. Birge, Phys. Rev. Lett. **104**, 137002 (2010).

[9] C. Klose, T. S. Khaire, Y. Wang, W. P. Pratt, N. O. Birge, B. J. McMorran, T. P. Ginley, J. A. Borchers, B. J. Kirby, B. B. Maranville, and J. Unguris, Phys. Rev. Lett. **108**, 127002 (2012).

[10] J. W. A. Robinson, F. Chiodi, M. Egilmez, G. B. Halasz, and M. G. Blamire, SCIENTIFIC REPORTS **2** (2012), 10.1038/srep00699.

[11] P. V. Leksin, N. N. Garif'yanov, I. A. Garifullin, Y. V. Fominov, J. Schumann, Y. Krupskaya, V. Kataev, O. G. Schmidt, and B. Büchner, Phys. Rev. Lett. **109**, 057005 (2012).

[12] F. S. Bergeret, A. F. Volkov, and K. B. Efetov, Phys. Rev. Lett. **86**, 4096 (2001).

[13] M. Eschrig and T. Loefwander, NATURE PHYSICS **4**, 138 (2008).

[14] F. S. Bergeret, A. F. Volkov, and K. B. Efetov, Rev. Mod. Phys. **77**, 1321 (2005).

[15] A. I. Buzdin, Rev. Mod. Phys. **77**, 935 (2005).

[16] S. Takei and V. Galitski, Phys. Rev. B **86**, 054521 (2012).

[17] F. S. Bergeret and I. V. Tokatly, Phys. Rev. Lett. **110**, 117003 (2013).

[18] Z. Yang, J. Wang, and K. Chan, Superconductor Science and Technology **22**, 055012 (2009).

[19] Z. Yang, J. Wang, and K. Chan, Journal of Physics: Condensed Matter **22**, 045302 (2010).

[20] E. A. Demler, G. B. Arnold, and M. R. Beasley, Phys. Rev. B **55**, 15174 (1997).

[21] M. Eschrig, Physics Today **64**, 43 (2011).

[22] B. A. Bernevig, J. Orenstein, and S.-C. Zhang, Phys. Rev. Lett. **97**, 236601 (2006).

[23] T. D. Stanescu and V. Galitski, Phys. Rev. B **75**, 125307 (2007).

[24] X. Liu and J. Sinova, Phys. Rev. B **86**, 174301 (2012).

[25] C. P. Weber, J. Orenstein, B. A. Bernevig, S.-C. Zhang, J. Stephens, and D. D. Awschalom, Phys. Rev. Lett. **98**, 076604 (2007).

[26] J. D. Koralek, C. P. Weber, J. Orenstein, B. A. Bernevig, S.-C. Zhang, S. Mack, and D. D. Awschalom, Nature **458**, 610 (2009).

[27] T. Champel, T. Löfwander, and M. Eschrig, Phys. Rev. Lett. **100**, 077003 (2008).

[28] D. S. Fisher and P. A. Lee, Phys. Rev. B **23**, 6851 (1981).

[29] C. J. Lambert, V. C. Hui, and S. J. Robinson, Journal of Physics: Condensed Matter **5**, 4187 (1993).

[30] J. Wang, Y. Wei, B. Wang, and H. Guo, Applied Physics Letters **79**, 3977 (2001).

[31] S. Datta, *Electronic Transport in Mesoscopic Systems (Cambridge Studies in Semiconductor Physics and Microelectronic Engineering)* (Cambridge University Press, 1997).

[32] See Supplemental Material [URL], which includes Ref. [33], for the derivation of transmission matrices $T_{\rm fm}^{\rm in}$, $T_{\rm soc}^{\rm in}$, $T_{\rm fm}^{\rm rf}$, $T_{\rm soc}^{\rm rf}$ and Andreev reflection matrix $R_{\rm ad}$ in 1D SC/FM/SOC junction, the property of the triplet pairing operators in 2D and the spatial of the evolution of the spin-triplet pairs in the SOC region.

[33] T. Schäpers, *Superconductor/semiconductor junctions*, Vol. 174 (Springer, 2001).

[34] C. Beenakker, in *Transport Phenomena in Mesoscopic Systems*, edited by H. Fukuyama and T. Ando, Vol. 109 (Springer, 1992).

[35] H. Tang, Z. Wang, and Y. Zhang, Zeitschrift fur Physik B Condensed Matter **101**, 359 (1997).

[36] J. K. J. Xin Liu and C.-X. Liu, To be published.

[37] K. D. Usadel, Phys. Rev. Lett. **25**, 507 (1970).

[38] J. Rammer, *Quantum Field Theory of Non-equilibrium States* (Cambridge University Press, 2007).

[39] Y.-J. Doh, J. a. van Dam, A. L. Roest, E. P. a. M. Bakkers, L. P. Kouwenhoven, and S. De Franceschi, Science **309**, 272 (2005).